Tim Arndt (Autor)

# Sloshing of Cryogenic Liquids in a Cylindrical Tank under normal Gravity Conditions

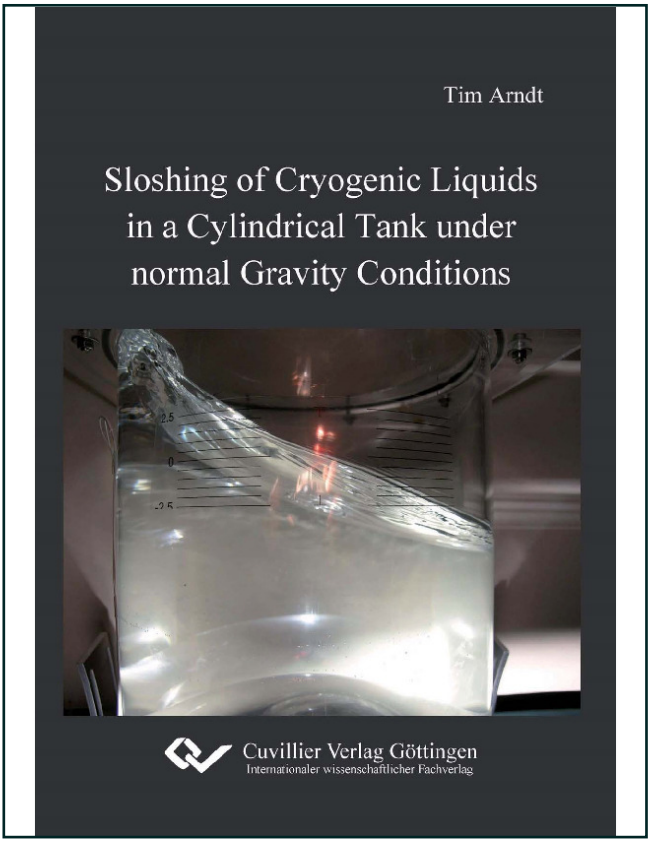


https://cuvillier.de/de/shop/publications/4

# Chapter 1

# INTRODUCTION

This work is dedicated to a - in general mostly unwanted - dynamic fluid behavior that is typically known as liquid sloshing. There exist many applications in civil and industrial engineering, in which this effect is of major interest. Frequently, liquid sloshing has been studied by designers of road and ship tankers as well as by geologists and architects to study its impact. Examples include large dam walls affected by underground motion and large liquid containers mounted on top of multistory buildings used as earthquake protection systems. Furthermore, the field of applications is enhanced by the aerospace industry where the understanding of liquid sloshing is of fundamental importance to design appropriate propellant tanks for spacecrafts. Liquid sloshing is defined as more or less periodical motion of the free liquid surface inside a closed reservoir[1]. It is provoked by any disturbances such as vibrations, acceleration changes or rolling and pitching movements of the tank. Depending on the excitation, this can cause different types of liquid motion including symmetric, asymmetric, swirling and chaotic sloshing modes.

This chapter starts with a compact review of the past. Afterwards, the application of cryogenic propellants including the risks compared to the utilization of storable liquids is discussed. The central part of this chapter deals with the principle question that shall be answered by this work. Furthermore, the state of the art related to cryogenic liquid sloshing is presented before the chapter closes with the motivation and the objectives for this work.

For centuries, one dream of Humankind is the exploration of the space - leaving Earth's atmosphere and beyond. Long before aeronautics and astronautics could be established as technical applications, these partially dreamy issues were primarily discussed by philosophers and litterateurs who cast their utopistic ideas into techno-romantic tales trying to influence the modern age world view. Well known ambassadors of this movement are Leonardo da Vinci, Giordano Bruno, Johannes Kepler, and Jules Verne, to name only a few of them. An example is provided in figure 1.1 showing the attempt to reach the moon by using a large gun bullet.

[1] Sloshing affects the liquid of a certain distance below the surface as well.

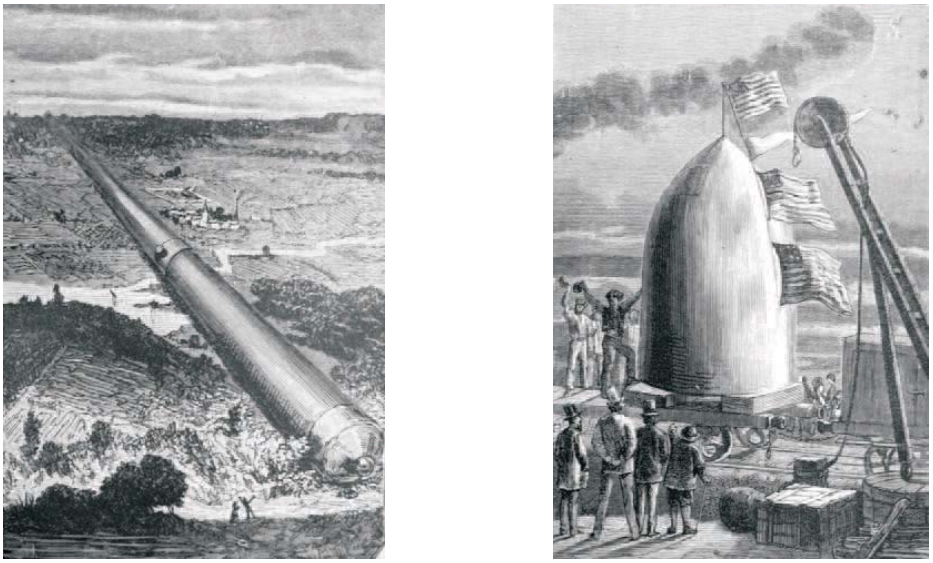

Figure 1.1: The shot to the Moon taken from the novel *From the Earth to the Moon* by Jules Verne written in 1865. The illustrations are taken from [56].

Driven by the cold war, space flights became of major interest during the 1950's and 1960's, when American and Soviet space programs were strongly supported by their governments, focusing on the manned exploration of Earth's orbit and the Moon. Highlights in this age were the first artificial earth satellite SPUTNIK launched by the USSR, the first manned space flight by YURI GAGARIN, and the American APOLLO program to perform the first manned landing on the Moon. Later, in the 1980's and 1990's, the reusable Space Shuttle and the International Space Station (ISS) shaped the face of modern astronautics. For unmanned missions, the European space launcher Ariane 5 advanced as one of the most successful carrier systems for satellite shipment into Earth's orbit.

Beating Earth's gravity field to reach the orbital position defines the main task of any launcher system that has been employed or will be designed in future. According to NEWTONs third law of motion, a rocket works on the principle providing a continuous ejection of hot gases in one direction to cause a thrust $\mathbf{F}_t$ and therefore a steady acceleration in the opposite direction. Thus, the momentum balance of the rocket must satisfy

$$\frac{d\,\mathbf{I}_{\text{tot}}}{dt} = \frac{d\,\mathbf{I}_r}{dt} + \frac{d\,\mathbf{I}_t}{dt} \tag{1.1}$$

where $\mathbf{I}_{\text{tot}}$ gives the total momentum. On the one side, the momentum of the rocket is defined as

$$\mathbf{I}_r\,(t) = m_r\,(t)\;\Delta\mathbf{u}_r\,(t)\;. \tag{1.2}$$

Here, $m_r$ is the actual rocket mass including the varying propellant mass and $\Delta\mathbf{u}_r$ is the change in rocket velocity. With the effective exhaust velocity $u_{ex}$, equation (1.2) gives in scalar notation

Table 1.1: The specific momentum $I_s$ of actual and outdated launcher systems [18, 44].

| launcher | stage/engine | propellant | kind | $I_s$ [s] |
|---|---|---|---|---|
| Saturn V | F-1 | LOX/RP-1 | semi-cryogenic | 265 |
| | J-2 | LOX/$LH_2$ | cryogenic | 424 |
| Ariane 4 (AR44 LP) | 2 | UH25/$N_2O_4$ | storable | 294 |
| | 3 | LOX/$LH_2$ | cryogenic | 444 |
| Ariane 5 | EPS | $N_2O_4$/MMH | storable | 231 |
| | ESC-A | LOX/$LH_2$ | cryogenic | 447 |
| Space Shuttle | SRB | Al/$NH_4ClO_4$ | solid | 295 |
| | SSME | LOX/$LH_2$ | cryogenic | 455 |

$$-u_{ex}\,\frac{dm_r}{dt} = m_r\,\frac{du_r}{dt} \tag{1.3}$$

leading to the well known Ziolkowky rocket equation

$$\Delta u_{12} = u_{ex}\ln\left[\frac{m_0}{m_1}\right] \tag{1.4}$$

where the initial total mass is denoted as $m_0$ and the final total mass is defined as $m_1$.

On the other side, the momentum emerging from the engine thrust $\mathbf{F}_t = v_e\,\dot{m}_p$ is defined as

$$\mathbf{I}_t\,(t) = \int_0^t \mathbf{F}_t\,dt. \tag{1.5}$$

According to equation (1.1), an payload extension requires a more powerful thrust provided by the engine. However, the specific momentum is a convenient measure to gauge the efficiency of rocket propellants. The specific momentum is defined as propellant weight related thrust, so that

$$I_s = \frac{|\mathbf{I}_t|}{a_z\,\int_0^t \dot{m}_p\,dt} \tag{1.6}$$

where $a_z = g$ is the gravitational acceleration on Earth and $\dot{m}_p$ is the actual propellant mass flow rate of the rocket. Although the specific momentum is a characteristic of the propellant system, its exact value will vary to some extent with the operating conditions and design of the rocket engine. The higher the specific momentum, the more energy is stored in the propellant and therefore the more payload can be carried by the launcher. For constant thrust and constant propellant flow, equation (1.6) simplifies yielding

$$I_s = \frac{|\mathbf{F}_t|}{g\,\dot{m}_p}. \tag{1.7}$$

(A) Ariane 5

(B) cryogenic upper stage

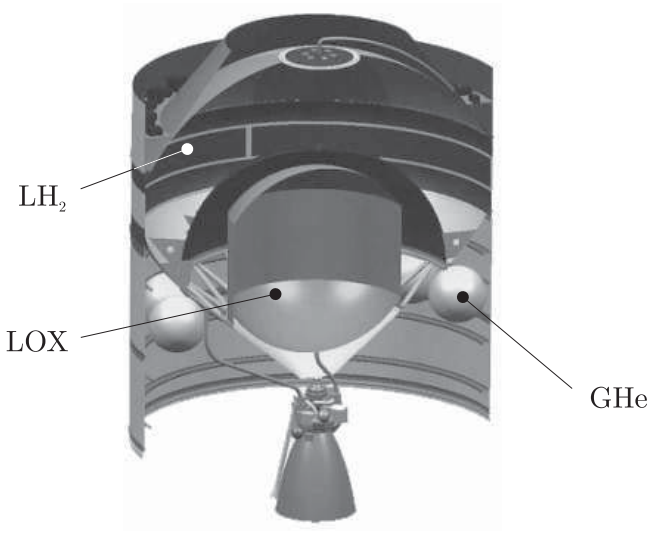


Figure 1.2: (A) The European space launcher Ariane 5 (illustration is provided by ESA). (B) Tank configuration of the cryogenic upper stage ESC-A [17] including the reservoirs for liquid hydrogen ($LH_2$), liquid oxygen (LOX) and gaseous helium (GHe).

For the general consideration of rocket propulsion systems during the flight where start and stop transients can be neglected, equation (1.7) is most appropriate.

Table 1.1 provides information about the specific momentum of actual and outdated launcher systems including Saturn V, Ariane 4, Ariane 5 and the Space Shuttle. In terms of $I_s$, obviously cryogenic systems provide the higher efficiency in comparison to storable propulsion systems driven typically by hydrazine[2] based propellants. For this reason, cryogenic engines are preferentially applied in rocket upper stages that are designed to be launched in lower orbits. However, a major disadvantage of cryogenic propellants is their notably low saturation temperature producing high amounts of boil-off. This represents a big challenge in terms of long time storage. The cryogenic upper stage ESC-A of the European space launcher Ariane 5 is shown in figure 1.2. Beside the tanks to store liquid oxygen (LOX) and helium (He), the axisymmetric reservoir for liquid hydrogen ($LH_2$) is the largest tank compartment of this stage. Initially, this tank is pressurized up to a certain system pressure that is in the order of 300 kPa, while the tank is approximately 95% full of cryogenic propellant.

During the ascent phase when the rocket executes several flight maneuvers such as rolling and pitching in order to reach Earth's orbit, liquid propellants tend to more or less periodic surface movements within the tank. Commonly, this is called liquid sloshing, which is typically caused by variations of the linear and angular acceleration in $x$, $y$ and $z$ direction. For most applications concerning propellant storage in rocket tanks, liquid sloshing is an undesired side effect causing unwanted mechanical and thermodynamical reactions in the rockets feed system. In this connection, two aspects are of major importance: damping and sudden pressure drops.

[2]Hydrazine is a storable nitrogen based propellant that is often utilized with nitric acid as oxidizer.

## Damping

Other than using solid or gaseous propellants, the utilization of liquid propellant imply the permanent occurrence of liquid motion that can not be completely prevented in rocket tanks. A notable property of liquid sloshing is the ability to dissipate energy as a result of viscous stresses within the liquid and between the liquid and the wall boundary. Commonly, this property is called damping. Among others, the damping characteristic of a liquid significantly influences the sloshing dynamics and in particular the maximum wave amplitude. In general, the higher the damping, the less dominant are the sloshing dynamics. Damping is directly connected to the liquid viscosity $\nu$, to the tank size $R$, to the acceleration level $a_z$ and for some extend to the tank fill level $H$. Since the damping level for a given tank/propellant combination is fixed during the ascent phase[3], the sloshing dynamics can be reduced by according tank design features such as the application of horizontal ring baffles. Ring baffles represent a substantial obstacle for the liquid motion during sloshing. However, the knowledge about the damping characteristics may help to improve the design of suitable tank solutions particularly for future upper stages.

## Pressure drops

By the utilization of cryogenic propellants, another important aspect is given by the impact of sloshing on the coupling between the heat and mass transfer at the phase interface between liquid and vapor. Background of this assumption is the fact that previously a sudden characteristic pressure drop occurred in the hydrogen tank of the Ariane 4 upper stage due to propellant sloshing during the ascent phase. As a matter of fact, a pressure drop might be critical compromising the structural stability of the tank. As mentioned before, the tank pressure is approximately $p = 300$ kPa. Due to certain flight maneuvers, the tank content is initiated to slosh. Within seconds, the pressure in the tank drops by 5 to 10%. It is assumed that the characteristic pressure drop phenomenon is caused by condensation effects that are provoked by the mixing of liquid at the free surface with liquid from the bulk.

Both aspects, the damping characteristics as well as the thermodynamic phenomena - such as the characteristic pressure drop - are of major importance since these effects may influence the tank design of future cryogenic upper stages. Furthermore, this might also be of interest by considering micro-gravity conditions particularly for engine shut-down and restart maneuvers in orbit. Here, propellant sloshing preferably may be considered as settling effect where the vector of the motion is different, but the occurring fluid dynamics as well as thermodynamic effects may appear in a similar manner.

[3]The tank is assumed to be filled to more than half of its volume with propellant.

## 1.1 State of the Art

The theoretical consideration of sloshing liquids in closed containers can be traced back to Lamb [40] who presented the mathematical description of oscillating surface waves in cylindrical tanks based on the potential theory using Bessel functions. Based on his approach, he could identify different sloshing modes showing a strong dependency on the excitation frequency. Viscous effects in cylindrical tanks with flat bottoms were considered firstly by Miles [46] as well as Case & Parkinson [22]. They assumed that viscous energy dissipation can be referred to a small boundary layer in the vicinity of the tank walls. In general, the dominant parameters that influence viscous damping effects in liquids can be characterized by the Galilei number defined as the ratio of gravitational forces to viscous forces so that $\mathbf{Ga} = a_z R^3/\nu^2$. However, an experimental proof was performed by Stephens *et al.* [55] conducting sloshing tests in a cylindrical tank using water. Mikishev & Dorozhkin [45] studied firstly spherical bottom geometries. Particularly for fill levels in the order of the tank size and below, they could identify a significant influence of the tank geometry on the damping characteristics of the liquid. Referring to the American aerospace agency, the most complete compendium in this period concerning liquid sloshing in rocket propellant tanks were composed by Bauer [15] as well as by Abramson [1] for NASA. Particularly the latter work contains approaches for analogous models to describe liquid sloshing. This includes spring mass and pendulum models where the liquid content is substituted by an oscillating mass point. Viscous properties were added by appropriate dashpot elements, so that the models are reduced to ordinary differential equations to describe the complex liquid system. Recently, this work was rewritten by Dodge [27] and later by Ibrahim [37], in which numerical methods for the analogous models were updated using more efficient simulation codes to compute the occurring sloshing forces and the natural frequencies particularly under the consideration of complex tank geometries.

With regard to the planned cryogenic upper stage for the European space launcher Ariane 5, experimental sloshing tests with storable liquids were conducted by Royon-Lebeaud *et al.* [51, 52]. They studied large amplitude sloshing and swirling waves in square-base and cylindrical tanks. Arndt & Dreyer [3, 6] performed sloshing experiments to test the influence of the bottom geometry on the damping characteristics of the liquid. They considered flat, spherical and convex bottom geometries using water to verify the damping models for storable liquids developed by Mikishev & Dorozhkin [45] and Stephens *et al.* [55]. The numerical results showed quite good agreement except for a flat bottom geometry where the numerical damping results performed with the commercial CFD software Flow3D[4] over-predict the experimental results by approximately a factor of 2.

In terms of cryogenic propellants, fundamental research was done on behalf of NASA in the 1960's and 1970's. One of the first cryogenic rocket engines that was developed by Rocket-

[4]FLOW3D Version 9.1.1. by Flow Science Inc.

DYNE is the J-2. Amongst others, this engine was applied on the third stage of the Saturn V rocket, the motor of the Apollo space program. The AS-203 experiment [57] that was performed on the V/S-IVB stage of a Saturn-I-B rocket, was conducted to verify the cryogenic propellant control system in consideration of the application on the Saturn V upper stage. Equipped with a variety of sensors, the main focus of this mission was to study cryogenic propellant characteristics during the ascent phase and in a low gravity environment.

To enhance the understanding of the thermodynamics within the framework of cryogenic propulsion, much work was done on fields of pressurization [10, 24, 50] and stratification [13, 14, 24, 42]. Recent numerical investigations in this area are conducted by GRAYSON *et al.* [31, 32], HIMENO *et al.* [35, 34] and LACAPERE *et al.* [39]. They studied the phase change at the free liquid surface in cryogenic liquids under the impact of sloshing.

MORAN *et al.* [48] performed full size ground sloshing experiments in pressurized spherical tanks using liquid hydrogen $LH_2$. Varying the excitation frequency, amplitude and ullage volume, the thermodynamic response under the impact of Earth's gravity could be characterized. It was found that particularly in the vicinity of the first natural frequency, sloshing effects have a major influence on the tank pressure development that may lead into ullage collapse. Furthermore, they could show that the pressure drop can be prevented by using helium as non-condensable pressurant gas. The pressure drop phenomenon on laboratory size scale was recently observed by LACAPERE *et al.* [39] studying laterally excited liquid nitrogen $LN_2$ in a $R = 0.095$ m cylindrical tank. The pressure drop could be numerically determined with a customized version of the commercial CFD software FLUENT. For the first asymmetric and symmetric sloshing modes, DAS & HOPFINGER [26] observed the characteristic pressure drop by using the engineering fluids FC-72 and HFE7000. This coheres with studies performed by HOPFINGER & DAS [36] who used FC-72 and HFE7000 as well. They could express the observed pressure variation in terms of an effective diffusion coefficient, the JACOB number and the temperature gradient in the boundary layer in the vicinity of the free surface. Experimental studies under variation of the pressurization are conducted by ARNDT *et al.* [7, 8] showing the influence of a non-condensable pressurant gas on the pressure drop phenomenon.

## 1.2 Motivation and Objectives

The motivation of this work is coupled to the development of a new cryogenic upper stage for the European space launcher Ariane 5. Particularly the layout of the propellant tank compartment to store liquid hydrogen ($LH_2$) may be influenced by the results that are discussed in this work. It is of fundamental importance to enhance the understanding of the fluid-dynamics of the cryogenic propellant and the thermodynamical effects that might occur under the impact of sloshing within the tank.

The understanding of the viscous damping for storable liquids such as water or engineering fluids is a widely explored field [6, 45, 52, 55]. In the current work, the damping model based on the Galilei number **Ga** will be tested for cryogenics and in particular for liquid nitrogen $LN_2$ as substitute for liquid hydrogen[5] $LH_2$. For a constant tank size, the fill level will be varied to emphasize the influence of the bottom geometry on the damping characteristics in an axis-symmetric tank with a spherical bottom shape.

Only few experimental investigations can be found in the literature concerning cryogenic propellant sloshing in gravity dominated environments that would reflect the conditions during the ascent phase [26, 39, 48]. Particularly the consideration of variable initial conditions represents a field of further investigation that may be important for the design of future upper stages.

The objectives of this work include the installation of an appropriate laboratory scale test facility in order to perform cryogenic sloshing tests with liquid nitrogen. Under the requirements of different initial conditions, the impact of the sloshing liquid shall be tested to study the changes of the corresponding thermodynamical conditions in the tank to identify the characteristic pressure drop phenomenon. For this purpose, the tank shall be pressurized by three different methods including

- *self-pressurization* where the tank is pressurized by means of the parasitic heat flow that continuously leaks into the system,
- *external nitrogen pressurization* where gaseous nitrogen from an external gas reservoir is fed into the tank, and
- *external helium pressurization* where gaseous helium from an external gas reservoir is fed into the tank.

The helium experiments are of particular interest, since helium is a non-condensable gas in a nitrogen environment. It is expected to reduce the pressure drop under the impact of sloshing. The obtained data is presented in nondimensional form in order to allow the up-scaling to other dimensions including previous experimental results as well as to enable predictions for the full size application. Previous data by Moran *et al.* [48], Lacapere [39] and Das & Hopfinger [26] performing experiments with higher initial pressures and other liquids are considered to confirm the actual results.

This work shall help to enhance the understanding of handling cryogenic liquids particularly when they are stored in upper stage rocket tanks. Furthermore, this work shows the limits of simple laboratory size experiments in order to simulate the complex full size geometry of upper stage tanks. Derived from actual results, it also suggest some motivation for future activities on this field.

[5] In the current case, the security guidelines for laboratory purpose of the University of Bremen prohibit the utilization of liquid hydrogen for quantities of approx. 20 liter without extensive modifications of the infrastructure.

# Chapter 2

# THEORETICAL BACKGROUND

This chapter is dedicated to the theoretical background to describe the occurring effects related to liquid sloshing. It starts with the introduction of the governing transport equations in accordance to explain the fluid dynamical problem. From these equations the corresponding characteristic numbers are derived to apply an adequate scaling. Furthermore, the fluid motion in the container is described by means of the potential theory. This theory is enhanced by a vortex potential function in order to consider the viscous property of the fluid as well [46, 45, 55]. The pressure drop phenomenon is theoretically described by an approach of Das & Hopfinger [26] by considering an effective diffusion coefficient within the liquid.

Figure 2.1 shows a typical cylindrical propellant tank with a spherical bottom shape as often found in actual and previous applications [1, 17, 27] with a liquid fraction ($L$) and an ullage ($U$).

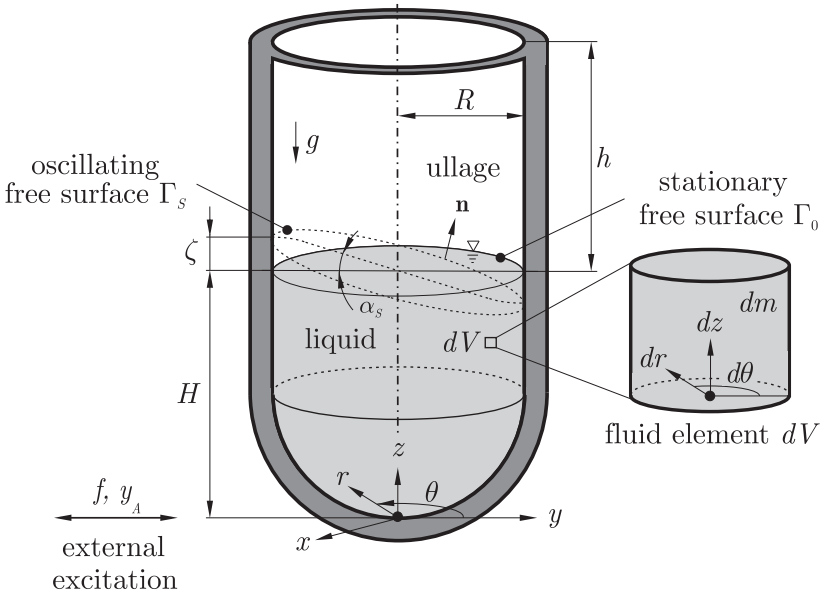


Figure 2.1: Schematic illustration of the tank including the definition of a single fluid element $dV$ of mass $dm$. The tank consists of a liquid and an ullage phase. The axes are defined in cylindrical and cartesian coordinates, while the origin is set to the tank bottom.

The tank is excited in $y$ direction, whereas $f$ is the frequency and $y_A$ is the amplitude of the oscillation. The $z$ axis points contrary to the gravity vector $\mathbf{g} = (0, 0, -g)^T$, while the $x$ direction points perpendicular to the excitation direction. Internally in terms of cylindrical coordinates, the radial direction is defined as $r$, the circumferential direction is $\theta$, and again, $z$ points from bottom to the top along the symmetry axis. The origin of the cylindrical coordinate system is set to the tank bottom. The stationary free surface is denoted as $\Gamma_0$, while the moving free surface is denoted as $\Gamma_S$. The normal vector perpendicular to the free surface is defined as $\mathbf{n}$.

The cylindrical tank has a radius of $R$ and is filled with liquid propellant up to a certain fill level $H$. Due to the excitation, the propellant content is forced into a sloshing motion, whereas the displacement of the oscillating liquid surface can be approximated by $\zeta = R \tan \alpha_s$ with respect to the stationary free surface. Here, $\alpha_s$ is the deflection angle of the free surface. The height of the ullage region is defined as $h$, so that the entire height of the tank is $L_T = H + h$. As described at the end of this chapter, the liquid motion can appear in different sloshing modes, which strongly depend on the excitation, the tank size, and the liquid properties.

## 2.1 Governing Equations

Typical fluid dynamical problems can be described by the three transport equations that are given by the conservation of mass, the conservation of momentum and the conservation of energy. In the following, these equations are introduced in general based on [19, 12, 23, 40, 49]. The local velocity of the fluid element $dV$ (see figure 2.1) with the mass $dm$ is defined as $\mathbf{u} = (u_r, u_\theta, u_z)^T$ in cylindrical coordinates. In order to satisfy the conventional definition, the liquid is considered as continuum with a free surface. In the following, the governing equations are introduced describing a one-phase system with liquid.

### 2.1.1 Conservation of Mass

The basic principle of the mass conservation includes that the mass $dm$ of the fluid element $dV$ with the density $\varrho$ is assumed to be constant. Therefore, the time variation of the mass equals the difference between inlet and outlet fluxes - or in general - the mass flow rate $\dot{m}$, so that

$$\frac{dm}{dt} = \dot{m}\,. \tag{2.1}$$

The time variation of the mass in the considered fluid element $dV$ is defined as

$$\frac{dm}{dt} = \frac{\partial}{\partial t} \int_V \varrho \, dV = \int_V \frac{\partial \varrho}{\partial t} \, dV\,. \tag{2.2}$$

The net mass flux along the contour $dA$ of the fluid element $dV$ is defined as

$$\dot{m} = - \oint_A \varrho \, u_i \, dA_i \tag{2.3}$$

where $u_i$ gives the $i^{\text{th}}$ velocity component of the velocity vector $\mathbf{u}$ at the fluid element contour $A_i$. Here, $i = 1$ corresponds to the radial direction $r$, $i = 2$ corresponds to the circumferential direction $\theta$, and $i = 3$ corresponds to the axial direction $z$. However, setting equation (2.2) and (2.3) into equation (2.1) gives the integral form of the mass balance

$$\int_V \frac{\partial \varrho}{\partial t} \, dV + \oint_A \varrho \, u_i \, dA_i = 0 \, . \tag{2.4}$$

Applying GAUSS theorem for volume calculation, the contour integral in equation (2.4) can be transformed into the volume integral

$$\int_V \frac{\partial \varrho}{\partial t} \, dV + \int_V \frac{\partial \varrho \, u_i}{\partial x_i} \, dV = 0 \, . \tag{2.5}$$

For infinitesimal volumes $V \to 0$, the differential form of the mass balance yields

$$\frac{\partial \varrho}{\partial t} + \nabla \cdot (\varrho \, \mathbf{u}) = 0 \, . \tag{2.6}$$

### 2.1.2 Conservation of Momentum

The conservation of momentum is derived from NEWTON's second law explaining that the time rate of the change of the linear momentum is proportional to the net forces $F_j$ acting on the fluid element $dV$ with the mass $dm$ yielding

$$\frac{d \, (m \, u_j)}{dt} = \sum F_j \tag{2.7}$$

where the linear momentum $P$ is defined as the product of the fluid mass $m$ and the local fluid velocity $\mathbf{u}$, so that $P \equiv m \, \mathbf{u}$. Thus, the left hand side of equation (2.7) reads

$$\frac{d \, (m \, u_j)}{dt} = \int_V \frac{\partial \, (\varrho \, u_j)}{\partial t} \, dV + \oint_A \varrho \, u_i \, u_j \, dA_i \tag{2.8}$$

consisting of a time dependent unsteady term and a term including the convective momentum transport. On the right hand side of equation (2.7), the net forces give

$$\sum F_j = \underbrace{- \oint_A p \, dA_j}_{(I)} + \underbrace{\oint_A \tau_{ij} \, dA_i}_{(II)} + \underbrace{\int_V \varrho \, f_j \, dV}_{(III)} \, , \tag{2.9}$$

where (I) gives the static pressure gradient, (II) gives the viscous momentum transport, and (III) gives the specific body forces $f_j$ acting on the fluid element. In consequence, the momentum balance in its integral form reads

$$\int_V \frac{\partial (\varrho\, u_j)}{\partial t}\, dV + \oint_A \varrho\, u_i\, u_j\, dA_i = -\oint_A p\, dA_j + \oint_A \tau_{ij}\, dA_i + \int_V \varrho\, f_j\, dV\,. \tag{2.10}$$

Applying the GAUSS theorem for volume calculation, the contour integrals can be converted into volume integrals. Then, equation (2.10) yields

$$\int_V \frac{\partial (\rho\, u_j)}{\partial t}\, dV + \int_V \frac{\partial (\rho\, u_i\, u_j)}{\partial x_i}\, dV = -\int_V \frac{\partial p}{\partial x_j}\, dV + \int_V \frac{\partial \tau_{ij}}{\partial x_i}\, dV + \int_V \varrho\, f_j\, dV\,. \tag{2.11}$$

For an incompressible Newtonian fluid, the viscous stress tensor $\tau_{ij}$ reduces to

$$\tau_{ij} = \mu \left[\frac{\partial u_j}{\partial x_i} + \frac{\partial u_i}{\partial x_j}\right] \tag{2.12}$$

with $\mu$ representing the dynamic viscosity. Then, the differential form of the momentum balance given in equation (2.11) can be rewritten in vector notation

$$\varrho \left[\frac{\partial \mathbf{u}}{\partial t} + (\mathbf{u}\cdot\nabla)\,\mathbf{u}\right] = -\nabla p + \mu\,\nabla^2\mathbf{u} + \varrho\,\mathbf{g} \tag{2.13}$$

where the specific body forces $f_j$ are replaced by the gravitational acceleration $\mathbf{g} = (0, 0, -g)^T$ representing the buoyancy term.

### 2.1.3 Conservation of Energy

According to the first law of thermodynamics for closed systems, the fluid element $dV$ can be balanced with the total internal energy $dU_{e,\,\mathrm{tot}}$ stored in the fluid, which is equal to the amount of energy added by heating $dQ$ as well as by mechanical work $dW$. Hereby, the system can be considered as an isochoric process since the volume of the tank is constant. Thus, the energy balance yields

$$\frac{dQ}{dt} + \frac{dW}{dt} = \frac{dU_{e,\,\mathrm{tot}}}{dt} + \dot{m}_{\mathrm{out}} \left[h_{e\,\mathrm{out}} + \frac{u_{\mathrm{out}}^2}{2} + g\,z\right] - \dot{m}_{\mathrm{in}} \left[h_{e\,\mathrm{in}} + \frac{u_{\mathrm{in}}^2}{2} + g\,z\right]\,. \tag{2.14}$$

For a closed system, the mass flow rates entering the tank $\dot{m}_{\mathrm{in}}$ and leaving the tank $\dot{m}_{\mathrm{out}}$ are zero. The energy term on the left hand side includes the internal energy (I) and the energy flux at the volume contour (II), so that

$$\frac{dU_{e,\,\mathrm{tot}}}{dt} = \underbrace{\int_V \frac{\partial (\varrho\, u_e)}{\partial t}\, dV}_{(I)} + \underbrace{\oint_A \varrho\, u_e\, u_i\, dA_i}_{(II)} \tag{2.15}$$

where $u_e = U_e/m$ is defined as specific internal energy with respect to the mass. While the internal energy is stored within the fluid, the energy flux at the volume contour corresponds to the mass that may be added or removed from the system. Furthermore, it is more convenient to express the energy stored in the fluid by introducing the enthalpy $H_e$ [11]. The enthalpy is defined as

$$H_e = U_e + pV \tag{2.16}$$

or in terms of the change of enthalpy

$$dH_e = dU_e + pdV + V dp\,. \tag{2.17}$$

However, the heat that is added can enter the system only through the volume contour yielding

$$\frac{dQ}{dt} = \oint_A \dot{q}_i \, dA_i \tag{2.18}$$

with $\dot{q} = \dot{Q}/A$ as specific heat flux. Mechanical work is only added indirectly to the system (excitation) and can therefore be neglected. According to Euler's approach, the external excitation does not need to be considered here. Thus,

$$\frac{dW}{dt} = 0\,. \tag{2.19}$$

Setting equation (2.15), (2.18), and (2.19) into equation (2.14) leads to the integral form of the energy balance given by

$$\int_V \frac{\partial\,(\varrho\, u_e)}{\partial t}\, dV + \oint_A \varrho\, u_e\, u_i\, dA_i = \oint_A \dot{q}_i\, dA_i\,. \tag{2.20}$$

Again, applying the Gauss theorem for volume calculation, the contour integrals can be converted into volume integrals yielding

$$\int_V \frac{\partial\,(\varrho\, u_e)}{\partial t}\, dV + \int_V \frac{\partial\,(\varrho\, u_e\, u_i)}{\partial x_i}\, dV = \int_V \frac{\partial \dot{q}_i}{\partial x_i}\, dV\,. \tag{2.21}$$

The right hand side term can be rewritten by means of Fourier's law of heat conduction $\dot{q}_i = -k\,\partial\vartheta/\partial x_i$. Regarding that the internal specific energy can be also expressed by the heat capacity for constant volume $c_v$, so that $u_e = c_v\,\vartheta$, the energy balance for a constant volume reads

$$\frac{\partial\,(\varrho\, c_v\, \vartheta)}{\partial t} + \frac{\partial\,(\varrho\, c_v\, \vartheta\, u_i)}{\partial x_i} = k\,\frac{\partial^2 \vartheta}{\partial x_i^2} \tag{2.22}$$

where $k$ is the thermal conductivity of the fluid. In vector notation, equation (2.22) can be rewritten

$$\varrho\, c_v \left[\frac{\partial \vartheta}{\partial t} + \mathbf{u}\cdot\nabla\vartheta\right] = k\,\nabla^2\vartheta\,. \tag{2.23}$$